Atmos. Chem. Phys. Discuss., 13, 32133–32173, 2013
www.atmos-chem-phys-discuss.net/13/32133/2013/
doi:10.5194/acpd-13-32133-2013

Atmospheric Chemistry and Physics Discussions

The effect of local sources on particle size and chemical composition and their role in aerosol-cloud interactions

H. Portin[1,2], A. Leskinen[1], L. Hao[2], A. Kortelainen[2], P. Miettinen[2], A. Jaatinen[2], A. Laaksonen[2,3], K. E. J. Lehtinen[1,2], S. Romakkaniemi[2], and M. Komppula[1]

[1]Finnish Meteorological Institute, P.O. Box 1627, 70211, Kuopio, Finland
[2]University of Eastern Finland, Department of Applied Physics, P.O. Box 1627, 70211, Kuopio, Finland
[3]Finnish Meteorological Institute, P.O. Box 503, 00101 Helsinki, Finland

Received: 15 November 2013 – Accepted: 21 November 2013 – Published: 9 December 2013

Correspondence to: H. Portin (harri.portin@fmi.fi)

Published by Copernicus Publications on behalf of the European Geosciences Union.

Abstract

The effects of local pollutant sources and particle chemical composition on aerosol–cloud interactions were investigated by measuring cloud interstitial and total aerosol size distributions, particle chemical composition and hygroscopic growth factors and cloud droplet size distributions on an observation tower, with a special focus on comparing clean air masses with those affected by local sources. The polluted air masses contained more particles than the clean air masses in all size classes, excluding the accumulation mode. This was caused by cloud processing, which was also observed for the polluted air but to a lesser extent. Some, mostly minor, differences in the particle chemical composition between the air masses were observed. The average size and number concentration of activating particles were quite similar for both air masses, producing average droplet populations with only minor distinctions. As a case study, a long cloud event was analyzed in detail regarding emissions from local sources, including a paper mill and a heating plant. Clear differences in the total and accumulation mode particle concentrations, particle hygroscopicity and chemical composition during the cloud event were observed. Particularly, larger particles, higher hygroscopicities and elevated amounts of inorganic constituents, especially SO_4, were linked with the pollutant plumes. In the air masses affected by traffic and domestic wood combustion, a bimodal particle hygroscopicity distribution was observed, indicating externally mixed aerosol. The variable conditions during the event had a clear impact on cloud droplet formation.

1 Introduction

Anthropogenic aerosol particles such as sulphates and carbonaceous aerosols have significantly increased the global mean burden of atmospheric aerosol compared to the pre-industrial times. Prediction of the current and future behaviour of the Earth's

ACPD
13, 32133–32173, 2013

climate system is complicated by the large uncertainties associated with the indirect effects of atmospheric aerosols (Lohmann and Feichter, 2005; IPCC 2013).

The indirect effect is characterized by the ability of aerosol particles to act as cloud condensation nuclei (CCN) or ice nuclei. More CCN means more and smaller droplets, which leads to the Twomey effect: higher cloud albedo and increased reflection of solar radiation (Twomey, 1977). Another consequence is the Albrecht effect: since droplets are smaller, the cloud liquid water path increases, precipitation development is weaker and the clouds are more persistent (Albrecht, 1989). However, this effect is more complicated than the Twomey effect, because, if cloud thermodynamics and dynamics are considered, the liquid water path may also decrease (Han et al., 2002).

Particle size, number concentration and chemical composition are the key aerosol properties in the cloud droplet activation process (Dusek et al., 2006; Hudson, 2007), which has been confirmed in studies based on satellite observations (Brenguier et al., 2003; Sekiguchi et al., 2003), model calculations (Menon et al., 2002; Rotstayn and Liu, 2005) and in-situ measurements (Coakley and Walsh, 2002; Wang et al., 2008). The effect of size and number concentration is well known (e.g. Vong and Covert, 1998; Henning et al., 2002; Komppula et al., 2005; Anttila et al., 2009), whereas the role of chemical composition is still under more investigation (e.g. Drewnick et al., 2007; Hao et al., 2013; Wu et al., 2013).

Using the ratio of the inorganic mass concentration to the total mass concentration (inorganic fraction, IO) as a measure of particle composition, Dusek et al. (2006) showed that ~ 80 % of the particle activation is explained by the particle size distribution and only 20 % by particle chemical composition. Kivekäs et al. (2009) found a positive correlation between activation efficiency and IO but IO was also correlated with accumulation mode particle concentration, making the separation of the effect of chemistry and particle size complicated.

Aerosol hygroscopicity defines how the particles grow at an elevated relative humidity and in the presence of a cloud. The distribution of the hygroscopic growth factor (GF_H), determined as the ratio of wet to dry aerosol particle diameter, can be used

ACPD
13, 32133–32173, 2013

as an indicator of the presence of less and more hygroscopic particles and thus, the aerosol mixing state. However, GF_H depends also on particle size (e.g. Sjogren et al., 2008; Kammermann et al., 2010; Fors et al., 2011), which is due to the Kelvin effect: for smaller particles, the partial pressure of water vapor on the more curved particle surface is higher, thus inhibiting the condensation of water. Furthermore, smaller particles are often less hygroscopic than larger particles, which are aged and possibly cloud processed.

So far, long-term in-situ observations on aerosol–cloud interactions are available only from a few measurement stations, e.g. the Global Atmospheric Watch stations at Pallas, Finland (e.g. Komppula et al., 2005) and Jungfraujoch, Switzerland (e.g. Henning et al., 2002) as well as the SMEAR (Station for Measuring Forest Ecosystem-Atmosphere Relations) IV station at Puijo, Finland (Leskinen et al., 2009; Portin et al., 2009; Hao et al., 2013; Ahmad et al., 2013). Puijo is located in a semiurban environment, which makes it easier to investigate the effects of local pollutant sources and therefore the effect of aerosols with different chemical composition on aerosol–cloud interactions. In this paper we present the results from two intensive measurement campaigns (Puijo Aerosol Cloud Experiment, PuCE 2010 and 2011) and provide new, detailed information about the effect of aerosols with different origins and chemical composition on the particle activation process.

2 Methods

2.1 Site description

The Puijo station resides on the top floor of the Puijo observation tower (62°54′32″ N, 27°39′31″ E, 306 m a.s.l., 224 m above the surrounding lake level), which is located in the city of Kuopio (105 000 inhabitants), in a semi-urban environment. Kuopio is situated in Eastern Finland, about 330 km to the Northeast from Helsinki (Fig. 1). A map of the area surrounding the tower is shown in Fig. 2, including the most important local

ACPD
13, 32133–32173, 2013

sources: a paper mill in the north, the city center in the southeast, a heating plant in the south and a highway in the east in north-south direction. Also, residential areas of different sizes surround the tower, with the biggest in the east and south and smaller in the southwest, west and northwest. All local sources are located within 10 km from the tower at approximately 200 m lower altitude than the measurement level (Table 1). A more detailed overview of the station and the surrounding area can be found in Leskinen et al. (2009).

2.2 Cloud events

A cloud event is considered to take place at Puijo when the visibility at the top of the tower drops below 200 m. Below this limit the cloud and particle activation properties have been observed to be stable, providing data with best possible quality (Portin et al., 2009). The clouds with a visibility above 200 m may already be non-uniform and the time resolution of the twin-inlet system is not enough to distinguish quickly varying particle properties. Furthermore, cloud events (or cloud event hours, see Sect. 2.4) are classified as rainy if the average rain intensity exceeds 0.2 mm h^{-1}. This classification is necessary, since rain drops remove both unactivated aerosol particles and cloud droplets, thus affecting the data.

2.3 Instrumentation

2.3.1 Twin inlet system

At the Puijo station the aerosol sample is collected with two separate inlets located on the top of the tower. The sample is drawn through the roof of the tower to the measurement devices which are located in a room on the top floor.

The total air inlet has a cutoff size of approximately 40 µm. The inlet and the upper part of the sampling line are heated to 40 °C. Thus, when the tower is in a cloud, the total air inlet will sample both the cloud droplets and the unactivated, interstitial aerosol

ACPD
13, 32133–32173, 2013

particles. The water from the droplets evaporates because of the heating, leaving only the residual particles. This way it is possible to observe the aerosol size distribution as it would be outside of the cloud.

The interstitial inlet has a PM_1 impactor (Digitel DPM_{10} for $1\,m^3\,h^{-1}$ flow rate) to prevent the cloud droplets from entering the sample line. When a cloud is present, this inlet samples only the interstitial aerosol since the cloud droplets are too large to enter the sampling line. During clear weather, both sampling lines measure the same aerosol distribution if the aerosol is not changing within 12 min measurement cycle. Between the main sampling lines and the measurement equipment is a valve system consisting of four controllable valves (Comparato, model Diamant, 2000) which are used to switch the measurement devices between the sampling lines in six-minute intervals.

2.3.2 Particle size distribution and number concentration

Particles in the size range of 7 to 800 nm were measured with a twin differential mobility particle sizer (twin-DMPS) (Winklmayr et al., 1991; Jokinen and Mäkelä, 1997). One DMPS measured between 7 to 49 nm with sheath and sample flows of 13.4 and $2\,L\,min^{-1}$, and the other from 27 to 800 nm with sheath and sample flows of 5.5 and $1\,L\,min^{-1}$, respectively. Flow checks were made periodically. The instrument was connected to the twin inlet system all the time and a full size distribution for both sampling lines was provided with a 12 min time resolution. The times of the measured size distributions from interstitial and total lines differ by six minutes, which has to be considered in the data analysis, normally by averaging over some time period. By comparing the size distributions between the sampling lines, it is possible to observe the size dependent cloud droplet activation of the particles.

In this study, we defined the nucleation mode particle concentration (N_{nuc}) as the concentration of particles with a diameter $D_p < 25$ nm. For Aitken mode particle concentration (N_{ait}) the corresponding size range is $25\,nm < D_p < 100\,nm$ and for the accumulation mode concentration (N_{acc})$D_p > 100$ nm. Moreover, D_{50} is defined as the

ACPD
13, 32133–32173, 2013

diameter above which at least 50 % of the particles have activated into cloud droplets (Komppula et al., 2005).

2.3.3 Cloud droplets

Cloud droplets were observed with a cloud droplet probe (CDP, Droplet Measurement Technologies) with a 10 s time resolution. The CDP measures the cloud droplet size distribution in the size range of 3 to 50 µm by classifying the droplets into 30 size bins according to the scattered light of a laser beam at a wavelength of 658 nm. The cloud droplet number concentration in each size bin is calculated by dividing the raw droplet counts with the volume of air passing through the sampling area of the laser beam. The instrument has a custom-built tubular inlet with an external pump to provide a constant sample flow (13 m s^{-1}, checked in the beginning of both campaigns). It is mounted on a swivel, which keeps the inlet facing the wind. The accuracy of the CDP is estimated to be 20–30 %, typical for other devices with the same detection principle (e.g. forward scattering spectrometer probe, FSSP) (Brenguier and Bourrianne, 1998). The size detection of the probe was proven with glass beads of 5 to 40 µm in diameter in the beginning of both campaigns. The CDP data was also used to estimate the cloud liquid water content (LWC) by calculating the total volume of the droplet population.

2.3.4 Particle chemical composition

The particle chemical composition was studied with an Aerodyne high resolution aerosol time-of-flight mass spectrometer (HR-ToF-AMS, DeCarlo et al., 2006). An aerodynamic lens focuses the particles into a narrow beam, which enters a vacuum, where the particles are flash-vaporized and ionizated. The ion fragments are detected by a time-of-flight mass spectrometer.

The aerosol mass spectrometer (AMS) provides the mass concentrations of organics, sulphate, nitrate, ammonium and chloride in the size range 40 nm < D_p < 1 µm. However, in this study the chloride data is omitted since the concentrations at Puijo

ACPD
13, 32133–32173, 2013

were negligible. The inorganic fraction (IO) is defined as the ratio of the inorganic mass concentration to the total mass concentration. Twin inlet data for the AMS is available for the whole 2011 campaign. In the 2010 campaign, the AMS was connected to the twin inlet system only for a period of 28 h for a case study (Hao et al., 2013), otherwise to the total line. To get uniform data from both campaigns, AMS data collected from the total line is used when discussing the whole 2010–2011 data set and twin-inlet data in the case study from the 2011 campaign.

2.3.5 Particle hygroscopicity

A hygroscopicity tandem differential mobility analyzer (H-TDMA, Joutsensaari et al., 2001) was used to observe the hygroscopic growth of aerosol particles during PuCE 2011. It was connected to the total air inlet in order to measure dried aerosol. The setup has a humidifier between the two DMAs. The first DMA selects particles with a certain dry size from the original polydisperse aerosol. In this study, the selected dry sizes were 80, 100 and 150 nm. The monodisperse aerosol enters the humidifier, which is set at 90 % relative humidity. The size distribution of the humid aerosol is measured with the second DMA. From this size distribution the average hygroscopic growth factor (GF_H, the ratio of wet to dry particle diameter) for a certain dry diameter is calculated. The instrument measures one dry size for five minutes, so a full cycle takes about 15 min. As the H-TDMA was operated only for a few days during the 2011 campaign, the data will be presented only for the case study.

Typical values of GF_H for 100 nm ambient aerosol particles (GF_{100}) vary from 1.0 to 1.5 (Sjogren et al., 2008). Black carbon is hydrophobic ($GF_H = 1.0$), organics are less hygroscopic ($GF_H \approx 1.2$) and anthropogenic particles with higher IO are more hygroscopic ($GF_H > 1.3$). The ratio between the number concentrations of more and less hygroscopic particles is defined as $R_{GF} = N_{GF>1.25}/N_{GF\leq1.25}$, where $N_{GF>1.25}$ and $N_{GF\leq1.25}$ are the number concentrations of particles with GF_H more than and less than or equal to 1.25, respectively. The limit 1.25 was chosen as it represented in most cases

ACPD
13, 32133–32173, 2013

the midpoint between the low GF_H and high GF_H modes of the hygroscopicity distributions of this study and the same limit was also used in Kammermann et al. (2010).

2.4 Data evaluation

As the first step of the data analysis, one-hour averages were calculated for the whole data set from both 2010 (20 September–22 October) and 2011 (26 September–31 October) campaigns, except for the CDP, for which the 10 s data were used. The averaging was done in order to even out discrepancies in the twin-DMPS size distributions between the sampling lines.

The hours with average visibility below 200 m were classified as cloud event hours. For the case study (Sect. 3.3), instead of hourly averages, the data were averaged over the different subperiods.

An hour was classified as a clear hour if the average relative humidity was below 80 % or the average height of the lowest cloud layer, measured by a ceilometer (Vaisala CT25K) located in a nearby weather station, was over 500 m (~ 300 m above the top of the tower). The choice to use these criteria instead of some high value for visibility was made because even at visibilities > 40 km, relative humidities higher than 90 % were sometimes observed, which is enough to have a noticeable effect on the twin inlet data.

To study the possible effects of the different local sources, the area surrounding the tower was divided into five sectors according to the local sources described in Sect. 2.1 (Table 1). The same sectors are also used in Leskinen et al. (2012). It must be noted that the local sources reside some 200 m lower, excluding the heating plant and paper mill, whose emission heights are about 80 and 128 m lower than the measurement altitude.

ACPD
13, 32133–32173, 2013

3 Results and discussion

3.1 Overview of cloud events

During PuCE 2010 and 2011, 39 cloud events were observed, ranging from short periods of 15 min to events lasting up to 31 h. In total, these events provided 156 cloud event hours (visibility < 200 m). The majority of the cloud event hours took place when the wind direction was from sector 3 (69 h) or sector 5 (50 h). It is very likely that the air masses coming from sector 5 are cleaner and possess some marine characteristics (Portin et al., 2009), whereas the air masses from sector 3 are affected by local sources. Thus, from now on, the results and discussion presented here will focus on the comparison of these two sectors, which will be referred as polluted (3) and clean (5) sectors, respectively.

3.2 Aerosol–cloud interactions for air masses with and without local pollutant sources

3.2.1 Particle size distribution

A summary of the aerosol properties for the sectors with and without local pollutant sources is shown in Table 2 along with the average values calculated from the whole data set. All the particle data discussed are from the total air inlet, if not mentioned otherwise. Also the standard error of the mean was calculated for the observations for the times corresponding to the one-hour averages. The values were calculated for clear (RH < 80 % or height of the lowest cloud > 500 m) (943 h in total) and cloudy conditions (156 h) during the campaigns. The corresponding average size distributions are shown in Fig. 3. The average particle number concentration (N_{tot}) in the air mass coming from the polluted sector in clear conditions (2930 cm^{-3}) was higher than that of the clean sector (2000 cm^{-3}) for all particle sizes. The mean total particle volume concentrations (V_{tot}) were 3.0 $\mu m^3 cm^{-3}$ and 0.80 $\mu m^3 cm^{-3}$ for the polluted and clean sec-

ACPD
13, 32133–32173, 2013

tors, respectively. Furthermore, the size distribution for the polluted sector was much broader, suggesting that the particles had originated from multiple sources.

In cloudy conditions, the mean N_{tot} decreased by 43 % for the polluted and by 51 % for the clean sector due to particles impacting into cloud droplets and wet removal. Scavenging was most significant for nucleation mode particles, leading to an increase in the geometric mean particle diameters (GMD) of the total aerosol (Fig. 3, Table 2). For the clean sector the GMD increased by 120 %, which is considerably more than the 16 % increase for the polluted sector. The V_{tot} was equal (2.5 $\mu m^3 cm^{-3}$) for both sectors in cloudy conditions. For the clean sector the V_{tot} in cloudy conditions was three times that in clear conditions. The differences in the particle populations of the two sectors can be explained by cloud processing: some of the smaller particles diffuse to droplets and trace gases convert to particulate matter within the droplets. This increases the size of activated particles and produces bimodal size distributions when the cloud droplets evaporate.

The cloud processing is often most evident in clean, marine aerosol (e.g. Hoppel et al., 1986; Frick and Hoppel, 1993; Mochida et al., 2011). At Puijo, cloud processing has been observed in the air masses from both sectors but it was more distinguishable in the air masses with possible marine characteristics arriving from the clean sector. For the polluted sector the effect of cloud processing was partly masked by the higher N_{tot}. A clear hump can be seen in the clean sector size distribution at around 200 nm (Fig. 3b), indicating cloud processing. The hump is also seen in the size distribution measured in clear conditions (Fig. 3a), meaning that the air masses have gone through cloud formation and processing on their way to Puijo. For the polluted sector, the hump can also be observed in both clear and cloudy conditions but it overlaps more with the Aitken mode.

3.2.2 Particle activation and cloud droplet size distribution

The average activated fractions as a function of particle diameter for the two sectors are shown in Fig. 4. For the polluted sector, even smaller particles activate and the activa-

ACPD
13, 32133–32173, 2013

tion curve is less steep than for the clean sector. The steepness of the activation curve gives information about the aerosol mixing state (Asmi et al., 2012). A steeper curve, like the one observed for the clean sector, is an indication of more internally mixed and more aged particles. A less steep curve means that aerosol from several sources with variable chemical composition and hygroscopic properties have been present, as is the case for the polluted sector. The number concentration of activated particles (N_{act}, calculated as the concentration difference between the total and interstitial sampling lines) differed by 21 % between the two sectors, being 210 cm^{-3} and 165 cm^{-3} for polluted and clean, respectively (Table 3). However, the size distributions of the activated particles were very similar for both sectors (Fig. 3b). The only difference was that the size distribution for the polluted sector was tilted towards smaller particle sizes, which also explains the difference in N_{act}.

The average droplet concentrations (N_d) were 293 and 266 cm^{-3} for the polluted and clean sectors, respectively. These numbers are comparable to N_{act} within the instrumental uncertainties of 20–30 %. The arithmetic mean droplet diameters (D_d) were 8.3 and 8.9 µm for the polluted and clean sectors, respectively (Table 3). Although these differences were small, this is just what one would expect based on the particle population properties of the two sectors. Higher N_{tot}, especially N_{acc}, of the polluted sector favors more and smaller droplets. The liquid water contents (LWC) were equal, 0.14 $g m^{-3}$, for both sectors.

3.2.3 Particle chemical composition

The mass concentrations of the chemical components for the two sectors are shown in Table 4. In clear conditions, the average concentrations of all measured constituents (organics, SO_4, NO_3, NH_4) were larger in the polluted air mass than in the clean air mass. In cloudy conditions, compared to the clear conditions, the NO_3 concentration was the same but the organics, SO_4, and NH_4 concentrations were lower by 18 %, 9 %, and 33 %, respectively, for the polluted sector. In the clean sector, the concentration of all constituents were higher by a factor of 2–6 compared to clear conditions. For NO_3

ACPD
13, 32133–32173, 2013

the concentration even exceeded that of the polluted sector and for NH_4 the concentrations were equal. The IO was 0.42–0.44 for both sectors and for both clear and cloudy conditions.

3.3 A case study on the effect of local sources on aerosol–cloud interactions

During PuCE 2011, a long cloud event took place between 22 October, 09:00 and 24 October, 05:15 LT, lasting in total 44 h. The wind direction, temperature and rain intensity varied considerably during the event. Also, different air masses and pollutant plumes from local sources were observed. Thus, it was possible to perform a detailed analysis on the effects of these variable conditions on aerosol–cloud interactions. The event could be divided into eight "sub-events" (Table 5). The time series of the most important weather and other parameters are shown in Figs. 5 and 6.

3.3.1 Rainy period

The rainy period, with a southerly wind from the polluted sector, a temperature of slightly over 0 °C and some rain (on average 0.8 mm h^{-1}), was characterized by the highest N_{tot} of all cloud periods (Table 6). This is mainly explained by a high N_{ait} (Fig. 7a), probably from fresh, anthropogenic emissions. N_{acc} was relatively high compared to the other periods, leading to a high droplet number concentration N_d with the smallest D_d of all the periods. Normally, the droplet size distribution was bimodal, with the first mode around 10 µm and second mode at ~ 16 µm (Fig. 7d). For this period, however, only the first mode was observed with a high amount of small droplets. LWC during this period was the lowest during the whole event, so it is possible that the droplet growth was limited by the availability of water.

The activated fraction of particles for this period remained low, even for the larger particles, reaching only 0.8 (Fig. 7c). This may also have been caused by the removal of droplets by rain, which affects the particle measurements. Unfortunately, as can be seen from Fig. 7a and c, the low amount of particles in the upper limit of DMPS mea-

ACPD
13, 32133–32173, 2013

surement range provides poor statistics, wrongly suggesting very low activated fractions for particles larger than 600 nm in diameter. Furthermore, the particle activation data in Fig. 7b and c suggests that also the smallest particles contributed to droplet formation. This inaccuracy was likely caused by the large variation in the concentrations of small particles, the 6 min time difference between the interstitial and total sampling lines and for some of the periods, the short averaging time. This has to be kept in mind when interpreting Fig. 7b and c and hence the data for particles smaller than 80 nm in diameter is illustrated with dashed lines.

The chemical composition of particles was dominated by organics, with the concentrations of other components remaining low (Table 7). The activated fraction of organics was the lowest for all periods. Also, the particles during this period had a low average hygroscopicity (Table 8) with very low R_{GF} indicating a strong contribution from the low GF_H particles. The growth factor distribution was clearly bimodal, especially for the 80 nm particles (Fig. 7e and f). It is likely that the nonhygroscopic mode consisted of particles containing organics or black carbon, some of which remained unactivated. The largest residential areas and a majority of the traffic in Kuopio are concentrated to the south from the tower. Both biomass burning and traffic related combustion aerosols are known to be less hygroscopic (Herich et al., 2009). This could also partly explain the low activated fraction.

3.3.2 Clean period

During the clean period, air masses were coming from the clean sector, there was no rain and the temperature dropped below 0 °C. The air was very clean, likely of marine origin and contained aged aerosol with low N_{tot} and N_{acc}. (Table 6). Also, there were no nucleation mode particles, which was already shown to be typical for this wind sector (Fig. 3). A low N_{acc} led to the lowest N_d of all the periods and a large D_d.

The mass concentrations of inorganic components were somewhat higher during this period compared to the rainy period (Table 7). Also, their activated fraction was higher, meaning that a larger fraction of them was found in the accumulation mode particles.

ACPD
13, 32133–32173, 2013

This suggests that the air mass was aged and had gone through some cloud processing, producing internally mixed aerosol before arriving to Puijo. This is also supported by high values for the hygroscopic growth factors (Table 8). The hygroscopicity distribution was dominated by the more hygroscopic mode, especially for the 100 and 150 nm particles as indicated by the high R_{GF} values. The R_{GF} of 100 and 150 nm particles was also strongly dependent on the concentration of SO_4. In the beginning of the period, SO_4 was almost absent but throughout the period, its mass fraction increased to 0.45. R_{GF} was around 2 and 6 in the beginning of the period but towards the end increased to 7 and 40 for 100 and 150 nm particles, respectively (Fig. 6c and 8). The average GF_{100} was 1.42, comparable with the Jungfraujoch free tropospheric aerosol, which is also aged and internally mixed (Sjogren et al., 2008; Kammermann et al., 2010).

3.3.3 Paper mill period

This short 30 min period was characterized by a heavy pollution plume from the nearby paper mill. There was no rain and the temperature was below 0 °C. The particle population properties differed greatly from those observed during the other periods. N_{tot} was very low but N_{acc} was elevated (Table 6). Due to the pronounced accumulation mode, a very high D_{50}, 202 nm, was observed, compared to the normal D_{50} at Puijo of around 120 nm, as was the case during the first two periods.

A time series of the cloud droplet data for the whole cloud event is shown in Fig. 6b. During the paper mill plume N_d increased momentarily, coinciding with a quick decrease in the average droplet size. This sharp change in the droplet population properties is mainly explained caused by the high N_{acc} but the possibility that the different chemical composition of particles also played a role cannot be excluded. The inorganic components all experienced a drastic increase, with SO_4 dominating the composition (Table 7). Growth factor distributions also showed elevated hygroscopicity for the high-GF_H mode, especially for the larger particles (Fig. 7f). However, the presence of a low-GF_H mode, probably containing soot particles, lowered the average hygroscopicities

ACPD
13, 32133–32173, 2013

during the plume (Table 8). For example, the average GF_{100} was 1.37, whereas for the high-hygroscopicity mode it was around 1.6.

3.3.4 Clean 2 period

In the beginning of this period, the wind direction shifted back to the north, fluctuating between the clean sector and sector 1, with no rain and a temperature of just below 0 °C. This period shared many similarities with the clean period. N_{tot} was even lower, nucleation mode particles were absent and a pronounced accumulation mode was observed (Fig. 7a, Table 6), indicating that strong cloud processing had taken place before the air mass arrived to Puijo.

The main difference compared with the clean period was an elevated inorganic mass concentration, largely due to 2–3 times higher SO_4 and NH_4 concentrations (Table 7). This indicates that the air mass has probably encountered some anthropogenic influence on its way to Puijo, but not from nearby sources. This had a clear influence on particle hygroscopicity, as seen from the high GF_H and R_{GF} values (Table 8) but not on cloud droplet activation. N_d was 10 % higher than during the clean period (Table 6) which is of similar magnitude as the difference in N_{acc} between the periods.

3.3.5 Heating plant period

The period started with a rapid shift in the wind direction from north to south and the polluted sector. The temperature was still slightly below 0 °C. At the same time, a heavy pollutant plume from the heating plant reached the tower. The particle population consisted of pronounced nucleation and accumulation modes (Fig. 7a). N_{acc} was the highest of all the periods, and the particles consisted mainly of SO_4 (Fig. 6c). Also, as the aerosol was highly acidic, the NO_3 concentration was very low. The plume also contained an exceptionally high amount of SO_2 (Fig. 6d), so it is likely that the majority of the SO_4 observed in the activated particles was formed from SO_2 as a result of cloud processing. However, SO_4 also dominated the composition of cloud interstitial parti-

ACPD
13, 32133–32173, 2013

cles. Since the smaller, inactivated particles are also liquid at high RH, it is possible that cloud processing from SO_2 to SO_4 took place also in the interstitial aerosol. Another explanation is that a part of the SO_4 particles was formed already at the heating plant.

The conclusions about particle activation parameters for this period have to be made carefully as the time resolution of the distribution scan is not good enough to capture the observed rapid changes in the aerosol properties. For example, D_{50} was very high, 273 nm, (Table 6) but this does not necessarily represent the actual size of the activating particles. The activated fraction of particles as a function of size (Fig. 7c) showed a bimodal behavior. Particles with a diameter of around 100 nm already started activating, similar to some other periods, but reached only an activation fraction of 0.4 at 150 nm. After this there is a dip in the curve as the heating plant particles started to affect the activation curve and produced a seemingly high D_{50}.

The GF_H distributions showed a clear bimodal behavior, with the high-GF_H mode slightly elevated by the heating plant particles. The low mode was also pronounced, and for 100 and 150 nm particles, similar to the observations during the rainy period, indicating emissions from traffic and residential areas. For 80 nm particles there was a clear increase in the low GF_H mode, indicating that the plume contained significant amounts of small particles with low hygroscopicity, likely soot. Since both hygroscopicity modes were affected by the plume, R_{GF} remained moderate. Unfortunately the CDP was frozen shortly after the beginning of the period, making analysis of the cloud properties impossible.

3.3.6 Southern 1 period

During this period, the conditions returned back to normal as the heating plant plume passed the tower. The temperature rose above 0 °C during the period and the wind direction was still from the south and the polluted sector. Similar nucleation and Aitken modes were present as during the heating plant plume (Fig. 7a). For the chemical components the concentrations were quite normal (Table 7). The GF_H distributions were

ACPD
13, 32133–32173, 2013

similar to those observed during the rainy period with bimodal shapes and moderate average GF_H and R_{GF} (Table 8). As the heating plant had no effect on data during the rainy period, it is likely that this was the case also here. Thus, southern 1 can be considered to represent normal "semipolluted" conditions for this sector when the effects of the heating plant and weather are minor. The CDP was still frozen part of the time, so no reliable droplet data is available.

3.3.7 Southern 2 period

After a short clear period, the tower was again covered in cloud with southerly wind and a temperature of above 0 °C. The aerosol during this period was moderately affected by the heating plant, indicated by the elevated SO_4 and SO_2 concentrations (Fig. 6). Also the concentration of organics was higher than during the earlier periods, which might already be related to the transportation of organic aerosol which was more pronounced during the next period, southern 3. The presence of two different kinds of aerosols had some effect on the activation of particles. The activated fraction curve was less steep than for most of the other periods and the size distribution of activated particles was broader (Fig. 6b and c). Also bimodal GF_H distributions and low R_{GF} indicated the presence of externally mixed aerosol. R_{GF} also (Fig. 8) correlated with SO_4 and SO_2 concentrations, with higher values in the middle of the period.

The cloud droplet size distribution was unimodal, similar to the rainy period. This suggests that the unimodality is an occasional feature for southerly clouds and not related to removal of droplets by rain as suggested for the rainy period. However, this does not exclude the possibility that rain removal of droplets was taking place during the rainy period. N_d during this period was higher despite a lower N_{acc} compared to the rainy period (Table 6).

ACPD
13, 32133–32173, 2013

3.3.8 Southern 3 period

During southern 3 period, wind was still blowing from the south. The period started with a drop in the mass concentration of SO_4 and in the concentration of SO_2 (Fig. 6). At the same time, the organic mass concentration increased to the highest value during the whole event (Table 7). The rise in the amount of organics was explained by an increase in N_{acc}, although N_{tot} remained lower than during other southern periods. As the chemical composition and N_{tot} showed little variance during the period (Fig. 6), this would suggest that the effect of local sources was minor. It is likely that these large organic particles were transported to Puijo from somewhere else.

These organic particles were also characterized by low hygroscopicity (Table 8). For 80 nm particles the hygroscopicity distribution was unimodal with one broad peak centered at $GF_H = 1.1$. Also for the 150 nm particles the low and high hygroscopicity peaks were broader than for the other periods. (Fig. 7e and f). It is possible that some of the larger particles remained unactivated because of this, as suggested by the unusually high D_{50} (Table 6). The availability of water was not a limiting factor. Although N_d was quite normal, the droplets were the largest and LWC the highest of all the periods.

3.4 Ratio of inorganics to total mass

Also shown in Table 7 is the IO from the AMS measurements for each of the periods. IO was the lowest for the rainy and southern 3 periods, 0.34 and 0.38, respectively, and higher for the clean, clean 2, southern 1 and southern 2 periods, 0.59, 0.64, 0.51 and 0.54, respectively. The highest IOs were observed during the paper mill and heating plant plumes, 0.85 and 0.87, respectively. The differences between the periods were considerably larger than those between the different air masses analyzed in Dusek et al. (2006) (0.18–0.42) and Kivekäs et al. (2009) (0.23–0.44). This further supports our findings that the local pollutant sources have a potential to affect aerosol–cloud interactions also through the particle chemical composition.

ACPD
13, 32133–32173, 2013

4 Summary and conclusions

Aerosol–cloud interactions were investigated during two intensive measurement campaigns at Puijo measurement site during autumns 2010–2011. The object was to find out the possible effects of local pollutant sources and particle chemical composition on aerosol–cloud interactions. The first approach was to compare data from two different wind direction sectors for the whole data set. One sector was considered to be clean, with air masses of mostly marine origin. The other sector was affected by local pollutant sources, including residential areas, traffic and a heating plant.

In clear conditions, the total particle number concentration and the accumulation mode concentration were higher for the polluted than for the clean sector. In cloudy conditions cloud processing took place, leading to lower particle concentrations. However, unlike for the polluted sector, the accumulation mode concentration increased for the clean sector, indicating stronger cloud processing. The In-cloud particle chemical composition was quite similar for both sectors. The main difference was a higher amount of sulfates for the polluted sector. Despite of some differences in the particle properties, the droplet activation behavior was surprisingly similar for the two sectors. The particles that activated were roughly of same size. For the polluted sector the average droplet concentration was higher and the average diameter smaller than for the clean sector but also these differences were minor.

The second approach was a case study of a cloud event with variable conditions. The wind was blowing from both the clean and polluted sectors and plumes from the local heating plant and paper mill were observed. The total and accumulation mode particle concentrations were clearly elevated for the polluted sector compared to the clean sector. This also created large differences in the droplet properties, with higher concentrations and smaller particle diameters for the polluted sector. Also the particle chemical composition, especially the ratio of inorganic to total mass concentration, varied considerably during the event.

ACPD
13, 32133–32173, 2013

Aged, cloud processed air masses from the clean sector typically resulted in an internally mixed, more hygroscopic aerosol with an inorganic fraction of ca. 0.6. With southerly winds, the particle hygroscopicity distributions were clearly bimodal, suggesting externally mixed aerosols. Likely sources for the less hygroscopic particles include local domestic wood combustion and traffic. The concentration of organics was higher, as indicated by the lower inorganic fraction, 0.3–0.5.

The paper mill plume was short in duration but a high accumulation mode particle concentration was observed, leading to a momentary increase in droplet concentration and a decrease in droplet size. The heating plant plume caused an even bigger increase in the accumulation mode concentration. In both plumes, elevated amounts of SO_4 and NH_4 were observed, leading to inorganic fractions of over 0.8. Unlike the paper mill plume, the heating plant plume also contained a large amount of SO_2. Thus, the SO_4 from the heating plant was formed from SO_2 as a result of cloud processing. For the paper mill plume, the SO_4 particles were either generated at the mill or then SO_2 was present to a lesser extent and was completely transformed into particulate SO_4 before arriving to Puijo. Another difference was the NO_3 concentration, which was elevated in the paper mill plume but very low in the heating plant plume due to highly acidic aerosol. In both plumes, elevated amounts of more hygroscopic particles were observed in addition to smaller, hydrophobic soot particles.

As a conclusion, the case study presented here supported and complemented the results from the sector comparison and the main results from these two methods can be summarized as follows: (1) the particle concentration in aged, cloud-processed, internally mixed and more hygroscopic air masses is low but a pronounced accumulation mode is present, leading to fewer cloud droplets with larger size. (2) Air masses affected by local sources contain more nucleation and Aitken mode particles with lower hygroscopicity. The aerosol is externally mixed with a higher inorganic content. The cloud droplets are smaller but more numerous. (3) Local point sources have the potential to affect aerosol–cloud interactions both through an increased particle concentration and through their effect on chemistry.

ACPD
13, 32133–32173, 2013

Acknowledgements. This work was partly supported by the Academy of Finland (Centre of Excellence, No 1118615 and decision number 267514), and the strategic funding of the University of Eastern Finland. L. Hao acknowledges the financial support of UEF Postdoc Research Foundation (No. 930275).

References

Ahmad, I., Mielonen, T., Grosvenor, D. P., Portin, H., Arola, A., Mikkonen, S., Kühn, T., Leskinen, A., Joutsensaari, J., Komppula, M., Lehtinen, K. E. J., Laaksonen, A., and Romakkaniemi, S.: Long-term measurements of cloud droplet concentrations and aerosol–cloud interactions in continental boundary layer clouds, Tellus B, 65, 20138, doi:10.3402/tellusb.v65i0.20138, 2013

Albrecht, B. A.: Aerosols, cloud microphysics, and fractional cloudiness, Science, 245, 1227–1230, 1989.

Anttila, T., Vaattovaara, P., Komppula, M., Hyvärinen, A.-P., Lihavainen, H., Kerminen, V.-M., and Laaksonen, A.: Size-dependent activation of aerosols into cloud droplets at a subarctic background site during the second Pallas Cloud Experiment (2nd PaCE): method development and data evaluation, Atmos. Chem. Phys., 9, 4841–4854, doi:10.5194/acp-9-4841-2009, 2009.

Asmi, E., Freney, E., Hervo, M., Picard, D., Rose, C., Colomb, A., and Sellegri, K.: Aerosol cloud activation in summer and winter at puy-de-Dôme high altitude site in France, Atmos. Chem. Phys., 12, 11589–11607, doi:10.5194/acp-12-11589-2012, 2012.

Brenguier, J.-L. and Bourrianne, T.: Improvements of droplet size distribution measurements with the fast-FSSP (Forward Scattering Spectrometer Probe), J. Atmos. Ocean. Tech., 15, 1077–1090, 1998.

Brenguier, J.-L., Pawlowska, H., and Schuller, L.: Cloud microphysical and radiative properties for parameterization and satellite monitoring of the indirect effect of aerosols on climate, J. Geophys. Res., 108, 8632, doi:10.1029/2002JD002682, 2003.

Coakley, J. A. and Walsh, C. D.: Limits to the aerosol indirect effect derived from obsevations of ship tracks, J. Atmos. Sci., 59, 668–680, 2002.

DeCarlo, P. F., Kimmel, J. R., Trimborn, A., Northway, M. J., Jayne, J. T., Aiken, A. C., Gonin, M., Fuhrer, K., Horvath, T., Docherty, K. S., Worsnop, D. R., and Jimenez, J. L.:

ACPD
13, 32133–32173, 2013

Field-deployable, high-resolution, time-of-flight aerosol mass spectrometer, Anal. Chem., 78, 8281–8289, 2006.
Drewnick, F., Schneider, J., Hings, S. S., Hock, N., Noone, K., Targino, A., Weimer, S., and Borrmann, S.: Measurement of ambient, interstitial, and residual aerosol particles on a mountaintop site in central Sweden using an aerosol mass spectrometer and a CVI, J. Atmos. Chem., 56, 1–20, 2007.
Dusek, U., Frank, G. P., Hildebrandt, L., Curtius, J., Schneider, J., Walter, S., Chand, D., Drewnick, F., Hings, S., Jung, D., Borrmann, S., and Andreae, M. O.: Size matters more than chemistry for cloud-nucleating ability of aerosol particles, Science, 312, 1375–1378, 2006.
Fors, E. O., Swietlicki, E., Svenningsson, B., Kristensson, A., Frank, G. P., and Sporre, M.: Hygroscopic properties of the ambient aerosol in southern Sweden – a two year study, Atmos. Chem. Phys., 11, 8343–8361, doi:10.5194/acp-11-8343-2011, 2011.
Frick, G. M. and Hoppel, W. A.: Airship measurements of aerosol size distributions, cloud droplet spectra, and trace gas concentrations in the marine boundary layer, B. Am. Meteorol. Soc., 74, 2195–2202, 1993.
Han, Q., Rossow, W. B., Zeng, J., and Welch, R.: Three different behaviors of liquid water path of water clouds in aerosol–cloud interactions, J. Atmos. Sci., 59, 726–735, 2002.
Hao, L. Q., Romakkaniemi, S., Kortelainen, A., Jaatinen, A., Portin, H., Miettinen, P., Komppula, M., Leskinen, A., Virtanen, A., Smith, J. N., Sueper, D., Worsnop, D. R., Lehtinen, K. E. J., and Laaksonen, A.: Aerosol chemical composition in cloud events by high resolution time-of-flight aerosol mass spectrometry, Environ. Sci. Technol., 47, 2645–2653, 2013.
Henning, S., Weingartner, E., Schmidt, S., Wendisch, M., Gäggeler, H. W., and Baltensperger, U.: Size-dependent aerosol activation at the high-alpine site Jungfraujoch (3580 m a.s.l.), Tellus B, 54, 82–95, 2002.
Herich, H., Kammermann, L., Friedman, B., Gross, D. S., Weingartner, E., Lohmann, U., Spichtinger, P., Gysel, M., Baltensperger, U., and Cziczo, D. J.: Subarctic atmospheric aerosol composition: 2. Hygroscopic growth properties, J. Geophys. Res., 114, D13204, doi:10.1029/2008JD011574, 2009.
Hoppel, W. A., Frick, G. M., and Larson, R. E.: Effect of nonprecipitating clouds on the aerosol size distribution in the marine boundary layer, Geophys. Res. Lett., 13, 125–128, 1986.

ACPD
13, 32133–32173, 2013

Hudson, J. G.: Variability of the relationship between particle size and cloud-nucleating ability, Geophys. Res. Lett., 34, L08801, doi:10.1029/2006GL028850, 2007.
IPCC: Climate change 2013: the Physical Science Basis, Intergovernmental Panel on Climate Change, Cambridge University Press, New York, 2013.
Jokinen, V. and Mäkelä, J. M.: Closed-loop arrangement with critical orifice for DMA sheath/excess flow system, J. Aerosol Sci., 28, 643–648, 1997.
Joutsensaari, J., Vaattovaara, P., Vesterinen, M., Hämeri, K., and Laaksonen, A.: A novel tandem differential mobility analyzer with organic vapor treatment of aerosol particles, Atmos. Chem. Phys., 1, 51–60, doi:10.5194/acp-1-51-2001, 2001.
Kammermann, L., Gysel, M., Weingartner, E., and Baltensperger, U.: 13-month climatology of the aerosol hygroscopicity at the free tropospheric site Jungfraujoch (3580 m a.s.l.), Atmos. Chem. Phys., 10, 10717–10732, doi:10.5194/acp-10-10717-2010, 2010.
Kivekäs, N., Kerminen, V.-M., Raatikainen, T., Vaattovaara, P., Laaksonen, A., and Lihavainen, H.: Physical and chemical characteristics of aerosol particles and cloud-droplet activation during the Second Pallas Cloud Experiment (Second PaCE), Boreal Environ. Res., 14, 515–526, 2009.
Komppula, M., Lihavainen, H., Kerminen, V.-M., Kulmala, M., and Viisanen, Y.: Measurements of cloud droplet activation of aerosol particles at a clean subarctic background site, J. Geophys. Res., 110, D06204, doi:10.1029/2004JD005200, 2005.
Leskinen, A., Portin, H., Komppula, M., Miettinen, P., Arola, A., Lihavainen, H., Hatakka, J., Laaksonen, A., and Lehtinen, K. E. J.: Overview of the research activities and results at Puijo semi-urban measurement station, Boreal Environ. Res., 14, 576–590, 2009.
Leskinen, A., Arola, A., Komppula, M., Portin, H., Tiitta, P., Miettinen, P., Romakkaniemi, S., Laaksonen, A., and Lehtinen, K. E. J.: Seasonal cycle and source analyses of aerosol optical properties in a semi-urban environment at Puijo station in Eastern Finland, Atmos. Chem. Phys., 12, 5647–5659, doi:10.5194/acp-12-5647-2012, 2012.
Lohmann, U. and Feichter, J.: Global indirect aerosol effects: a review, Atmos. Chem. Phys., 5, 715–737, doi:10.5194/acp-5-715-2005, 2005.
Menon, S., Del Genio, A. D., Koch, D., and Tseloudis, G.: GCM simulations of the aerosol indirect effect: sensitivity to cloud parameterization and aerosol burden, J. Atmos. Sci., 59, 692–713, 2002.
Mochida, M., Nishita-Hara, C., Furutani, H., Miyazaki, Y., Jung, J., Kawamura, K., and Uematsu, M.: Hygroscopicity and cloud condensation nucleus activity of marine

ACPD
13, 32133–32173, 2013

aerosol particles over the western North Pacific, J. Geophys. Res., 116, D06204, doi:10.1029/2010JD014759, 2011.
Portin, H., Komppula, M., Leskinen, A., Romakkaniemi, S., Laaksonen, A., and Lehtinen, K. E. J.: Observations of aerosol–cloud interactions at Puijo semi-urban measurement station, Boreal Environ. Res., 14, 641–653, 2009.
Rotstayn, L. D. and Liu, Y.: A smaller global estimate of the second indirectaerosol effect, Geophys. Res. Lett., 32, L05708, doi:10.1029/2004GL021922, 2005.
Sekiguchi, M., Nakajima, T., Suzuki, K., Kawamoto, K., Higurashi, A., Rosenfeld, D., Sano, I., and Mukai, S.: A study of the direct and indirect effects of aerosols and cloud parameters, J. Geophys. Res., 108, 4699, doi:10.1029/2002JD003359, 2003.
Sjogren, S., Gysel, M., Weingartner, E., Alfarra, M. R., Duplissy, J., Cozic, J., Crosier, J., Coe, H., and Baltensperger, U.: Hygroscopicity of the submicrometer aerosol at the high-alpine site Jungfraujoch, 3580 m a.s.l., Switzerland, Atmos. Chem. Phys., 8, 5715–5729, doi:10.5194/acp-8-5715-2008, 2008.
Twomey, S.: The influence of pollution on the shortwave albedo of clouds, J. Atmos. Sci., 34, 1149–1152, 1977.
Vong, R. J. and Covert, D. S.: Simultaneous observations of aerosol and cloud droplet size spectra in marine stratocumulus, J. Atmos. Sci., 55, 2180–2190, 1998.
Wang, J., Lee, Y.-N., Daum, P. H., Jayne, J., and Alexander, M. L.: Effects of aerosol organics on cloud condensation nucleus (CCN) concentration and first indirect aerosol effect, Atmos. Chem. Phys., 8, 6325–6339, doi:10.5194/acp-8-6325-2008, 2008.
Winklmayr, W., Reischl, G. P., Linder, A. O., and Berner, A.: A new electromobility spectrometer for the measurement of aerosol size distribution in the size range 1 to 1000 nm, J. Aerosol Sci., 22, 289–296, 1991.
Wu, Z. J., Poulain, L., Henning, S., Dieckmann, K., Birmili, W., Merkel, M., van Pinxteren, D., Spindler, G., Müller, K., Stratmann, F., Herrmann, H., and Wiedensohler, A.: Relating particle hygroscopicity and CCN activity to chemical composition during the HCCT-2010 field campaign, Atmos. Chem. Phys., 13, 7983–7996, doi:10.5194/acp-13-7983-2013, 2013.

ACPD
13, 32133–32173, 2013

Table 1. Sectors used for data classification and a list of local sources.

	Sector	Source	Direction and distance from the tower
1	0–45°	Paper mill Highway	35°, 5 km 6–45°, > 1.4 km
2	45–155°	City center Residential areas Highway	120–155°, 1.6–3.2 km 45–120°, 1.2–4 km 45–155°, 1–1.4 km
3	155–215°	Heating plant Residential areas Highway	160°, 3.5 km 155–215°, 3.4–10 km 155–192°, > 1 km
4	215–245°	Residential areas	215–245°, 3.4–4 km
5	245–360°	Residential areas	245–360°, 1.5–3.5 km

ACPD
13, 32133–32173, 2013

Table 2. Average values and standard deviations of total particle number concentration (N_{tot}), geometric mean particle diameter (GMD), total particle volume concentration (V_{tot}), number concentrations of nucleation, Aitken and accumulation mode particles (N_{nuc}, N_{ait}, N_{acc}) and ratio N_{ait}/N_{acc}. Values are calculated from the twin-DMPS data for the sectors with and without local pollutant sources, for the whole data set and for both clear and cloudy conditions. Data are from the total sampling line.

sector	N_{tot} (cm^{-3})		GMD (nm)		V_{tot} ($\mu m^3 cm^{-3}$)		N_{nuc} (cm^{-3})		N_{ait} (cm^{-3})		N_{acc} (cm^{-3})		N_{ait}/N_{acc}	
	clear	cloud	clear	cloud	clear	cloud	clear	cloud	clear	cloud	clear	cloud	clear	cloud
polluted	2930 ±2030	1680 ±1020	44 ±19	51 ±24	3.0 ±2.2	2.5 ±2.7	1170 ±1780	511 ±580	1180 ±525	727 ±436	580 ±384	438 ±490	3.2 ±3.0	2.8 ±2.3
clean	2000 ±1510	972 ±771	35 ±20	77 ±30	0.80 ±0.94	2.5 ±2.3	1040 ±1250	126 ±258	812 ±578	498 ±404	146 ±142	349 ±291	9.2 ±8.8	2.5 ±2.6
all	2480 ±2440	1530 ±1100	39 ±21	59 ±29	1.6 ±1.8	2.6 ±2.4	1070 ±2120	443 ±624	1000 ±652	669 ±452	311 ±312	416 ±392	6.6 ±7.0	2.6 ±2.6

ACPD
13, 32133–32173, 2013

Table 3. Average values and standard deviations of number concentration of activated particles (N_{act}, calculated as the concentration difference between the total and interstitial lines), cloud droplet number concentration (N_d), droplet diameter (D_d) and liquid water content (LWC) in cloudy conditions for the sectors with and without local pollutant sources and for the whole data set.

sector	N_{act} (cm^{-3})	N_d (cm^{-3})	D_d (μm)	LWC ($g\,m^{-3}$)
polluted	210 ± 148	293 ± 159	8.3 ± 2.3	0.14 ± 0.13
clean	165 ± 126	266 ± 124	8.9 ± 2.2	0.14 ± 0.09
all	209 ± 186	285 ± 168	8.9 ± 2.3	0.15 ± 0.12

ACPD
13, 32133–32173, 2013

Table 4. Average mass concentrations and standard deviations of the chemical constituents measured by the AMS for the sectors with and without local pollutant sources, for the whole data set and for both clear and cloudy conditions. Data are from the total sampling line.

sector	Organics ($\mu g\,m^{-3}$)		SO_4 ($\mu g\,m^{-3}$)		NO_3 ($\mu g\,m^{-3}$)		NH_4 ($\mu g\,m^{-3}$)		Inorg/total	
	clear	cloud	clear	cloud	clear	cloud	clear	cloud	clear	cloud
polluted	2.17 ±2.1	1.79 ±2.25	1.19 ±1.1	1.08 ±1.26	0.21 ±0.27	0.19 ±0.18	0.40 ±0.42	0.27 ±0.29	0.42 ±0.12	0.44 ±0.18
clean	0.48 ±2	1.61 ±1.1	0.27 ±0.34	0.69 ±0.55	0.04 ±0.02	0.24 ±0.15	0.05 ±0.07	0.27 ±0.22	0.42 ±0.29	0.43 ±0.17
all	1.22 ±3.2	1.62 ±1.9	0.71 ±0.93	0.92 ±1.06	0.13 ±0.22	0.21 ±0.17	0.22 ±0.35	0.28 ±0.26	0.43 ±0.22	0.46 ±0.18

ACPD
13, 32133–32173, 2013

Table 5. Summary of the different periods during the cloud event observed in 22–24 October 2011.

	period	time	sector	Temperature (°C)	special characteristics
1	rainy	22 Oct 09:00–12:00	polluted	0.9	rainy
2	clean	22–23 Oct 22:00–05:45	clean	−0.3	none
3	paper mill	23 Oct 05:45–06:15	1	−0.6	paper mill plume
4	clean 2	23 Oct 06:40–08:50	clean, 1	−0.7	none
5	heating plant	23 Oct 09:45–13:00	polluted	−0.5	heating plant plume
6	southern 1	23 Oct 14:00–15:45	polluted	0	none
7	southern 2	23 Oct 17:45–23:05	polluted	1.6	none
8	southern 3	23–24 Oct 23:05–05:15	polluted	3.6	none

ACPD
13, 32133–32173, 2013

Table 6. Average values and standard deviations of total particle number concentration (N_{tot}), geometric mean particle diameter (GMD), accumulation mode particle number concentration (N_{acc}), diameter of 50 % activation (D_{50}), cloud droplet number concentration (N_d), droplet diameter (D_d) and liquid water content (LWC) for the different periods of the cloud event observed on 22–24 October 2011.

period	N_{tot} (cm^{-3})	GMD (nm)	N_{acc} (cm^{-3})	D_{50} (nm)	N_d (cm^{-3})	D_d (µm)	LWC ($g m^{-3}$)
rainy	2200 ± 576	35 ± 3	149 ± 37	119 ± 9	219 ± 69	9.2 ± 1.1	0.11 ± 0.04
clean	451 ± 195	49 ± 8	62 ± 18	112 ± 20	138 ± 32	12.2 ± 1.9	0.17 ± 0.08
paper mill	357 ± 74	82 ± 11	139 ± 44	202 ± 106	240 ± 53	10.9 ± 0.8	0.22 ± 0.04
clean 2	214 ± 22	77 ± 5	83 ± 9	146 ± 28	152 ± 30	11.8 ± 0.6	0.16 ± 0.04
heating plant*	1130 ± 499	35 ± 9	169 ± 50	273 ± 89	–	–	–
southern 1*	987 ± 199	29 ± 7	114 ± 19	118 ± 17	–	–	–
southern 2	801 ± 388	40 ± 10	123 ± 26	118 ± 30	234 ± 49	10.0 ± 1.0	0.15 ± 0.04
southern 3	754 ± 135	59 ± 7	169 ± 41	163 ± 20	197 ± 50	12.4 ± 1.7	0.30 ± 0.09

* Cloud droplet probe frozen during these periods, data missing or otherwise unreliable.

ACPD
13, 32133–32173, 2013

Table 7. Average mass concentrations and standard deviations from the total line, activated concentration (difference in the mass concentration between total and interstitial lines) and activated fraction of chemical constituents for the different periods of the cloud event observed on 22–24 October 2011.

period	Organics			SO_4 ($\mu g m^{-3}$)			NO_3 ($\mu g m^{-3}$)			NH_4 ($\mu g m^{-3}$)			inorg./ total
	tot ($\mu g m^{-3}$)	act ($\mu g m^{-3}$)	act frac	tot ($\mu g m^{-3}$)	act ($\mu g m^{-3}$)	act frac	tot ($\mu g m^{-3}$)	act ($\mu g m^{-3}$)	act frac	tot ($\mu g m^{-3}$)	act ($\mu g m^{-3}$)	act frac	
rainy	0.72 ±0.22	0.45 ±0.26	0.62 ±0.22	0.16 ±0.06	0.13 ±0.07	0.78 ±0.14	0.15 ±0.05	0.12 ±0.05	0.79 ±0.11	0.05 ±0.03	0.05 ±0.03	0.94 ±0.09	0.34 ±0.07
clean	0.42 ±0.28	0.29 ±0.34	0.71 ±0.52	0.20 ±0.15	0.18 ±0.15	0.91 ±0.15	0.23 ±0.05	0.21 ±0.05	0.91 ±0.07	0.10 ±0.05	0.10 ±0.05	0.98 ±0.06	0.59 ±0.14
paper mill	0.69 ±0.16	0.58 ±0.2	0.84 ±0.17	2.46 ±0.86	2.2 ±0.90	0.90 ±0.12	0.42 ±0.01	0.35 ±0.07	0.85 ±0.16	0.99 ±0.31	0.90 ±0.33	0.91 ±0.12	0.85 ±0.02
clean 2	0.61 ±0.12	0.50 ±0.22	0.82 ±0.30	0.57 ±0.08	0.49 ±0.09	0.86 ±0.08	0.27 ±0.04	0.24 ±0.04	0.88 ±0.05	0.24 ±0.04	0.23 ±0.04	0.95 ±0.04	0.64 ±0.04
heating plant	0.69 ±0.30	0.56 ±0.34	0.80 ±0.26	4.43 ±1.62	3.4 ±1.81	0.77 ±0.2	0.08 ±0.08	0.06 ±0.08	0.78 ±0.29	0.52 ±0.34	0.46 ±0.36	0.87 ±0.23	0.87 ±0.07
southern 1	0.72 ±0.17	0.57 ±0.29	0.80 ±0.34	0.47 ±0.19	0.44 ±0.19	0.95 ±0.07	0.14 ±0.03	0.13 ±0.03	0.89 ±0.05	0.13 ±0.05	0.13 ±0.05	0.99 ±0.01	0.51 ±0.09
southern 2	0.81 ±0.23	0.66 ±0.30	0.82 ±0.25	0.66 ±0.28	0.62 ±0.29	0.93 ±0.08	0.15 ±0.07	0.13 ±0.07	0.89 ±0.07	0.16 ±0.06	0.16 ±0.06	0.99 ±0.02	0.54 ±0.08
southern 3	1.28 ±0.36	0.83 ±0.43	0.65 ±0.21	0.46 ±0.25	0.37 ±0.26	0.81 ±0.19	0.17 ±0.08	0.13 ±0.08	0.79 ±0.17	0.12 ±0.10	0.11 ±0.11	0.94 ±0.21	0.38 ±0.06

ACPD
13, 32133–32173, 2013

Table 8. Average values and standard deviations of particle hygroscopic growth factors GF_H and the ratios between more and less hygroscopic particle number concentrations, $R_{GF} = N_{GF>1.25}/N_{GF\leq1.25}$ for the different periods of the cloud event observed on 22–24 October 2011.

	80 nm		100 nm		150 nm	
period	GF_H	R_{GF}	GF_H	R_{GF}	GF_H	R_{GF}
rainy	1.16 ± 0.04	0.42 ± 0.12	1.25 ± 0.04	1.43 ± 0.45	1.33 ± 0.02	2.69 ± 0.63
clean	1.24 ± 0.05	0.79 ± 0.39	1.42 ± 0.08	4.90 ± 2.47	1.55 ± 0.08	26.0 ± 16.4
paper mill	1.17 ± 0.02	0.44 ± 0.07	1.37 ± 0.01	2.06 ± 0.34	1.56 ± 0.06	23.9 ± 10.9
clean 2	1.28 ± 0.04	1.29 ± 0.44	1.45 ± 0.03	9.13 ± 4.29	1.53 ± 0.02	5.15 ± 1.56
heating plant	1.24 ± 0.11	1.09 ± 1.02	1.36 ± 0.09	3.74 ± 3.79	1.48 ± 0.03	8.75 ± 6.83
southern 1	1.22 ± 0.05	0.92 ± 0.41	1.32 ± 0.12	3.73 ± 3.84	1.39 ± 0.03	12.8 ± 8.93
southern 2	1.20 ± 0.06	0.62 ± 0.31	1.34 ± 0.07	2.50 ± 1.29	1.43 ± 0.04	3.03 ± 1.18
southern 3	1.17 ± 0.03	0.36 ± 0.15	1.21 ± 0.03	0.88 ± 0.32	1.34 ± 0.05	7.64 ± 2.78
rainy	1.16 ± 0.04	0.42 ± 0.12	1.25 ± 0.04	1.43 ± 0.45	1.33 ± 0.02	2.69 ± 0.63

ACPD
13, 32133–32173, 2013

Fig. 1. Location of Kuopio.

ACPD
13, 32133–32173, 2013

The effect of local sources on aerosol-cloud interactions

H. Portin et al.

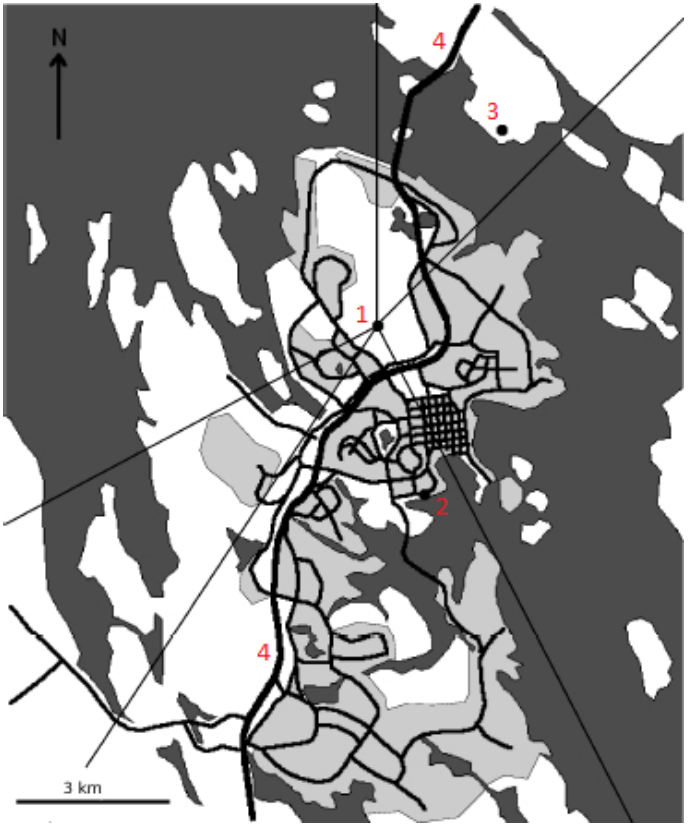

Fig. 2. Map of Kuopio area. Marked in the figure are Puijo (1), a heating plant (2), a paper mill (3) and a highway (4). Dark grey color presents lakes, light grey residential areas and white forests. Also shown are five sectors used in the data analysis to distinguish the effect of local sources (described in Sect. 2.4).

ACPD
13, 32133–32173, 2013

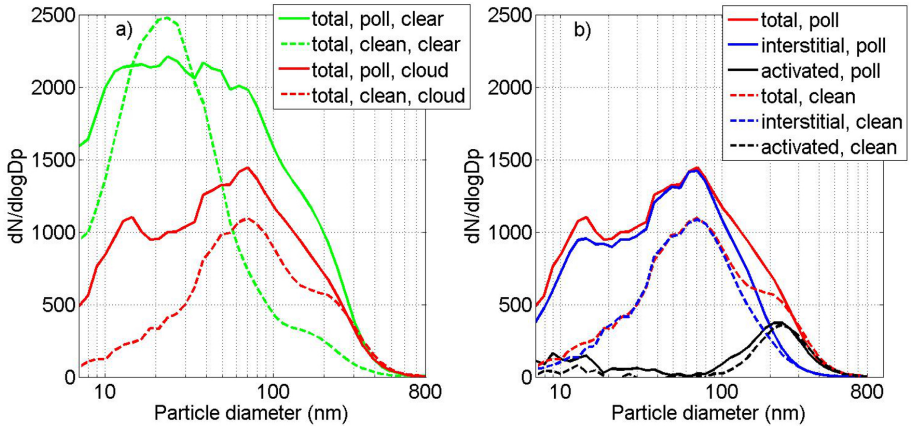

Fig. 3. (a) Average total particle size distributions in both clear and cloudy conditions and **(b)** average total, interstitial, and activated particle size distributions for polluted and clean sectors in cloudy conditions.

ACPD
13, 32133–32173, 2013

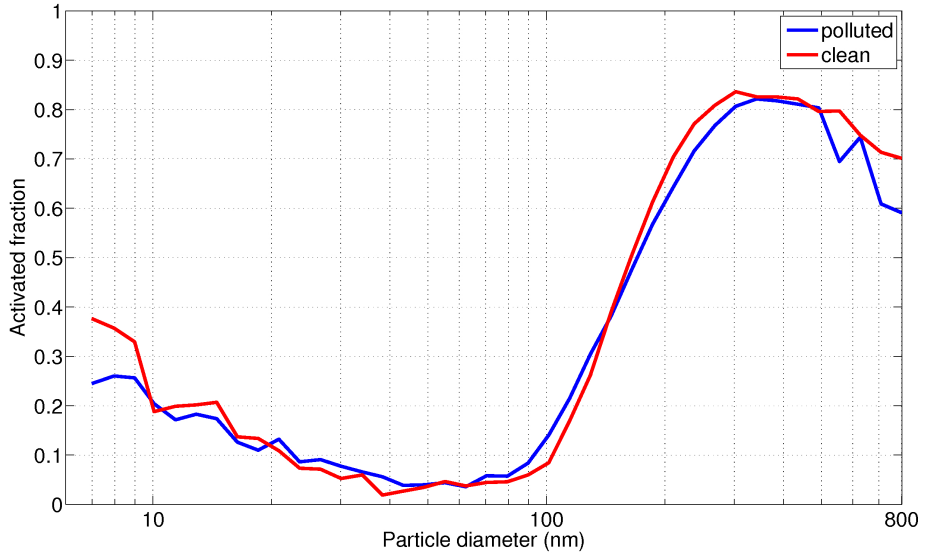

Fig. 4. Average activated fractions as a function of particle diameter for polluted and clean sectors.

ACPD
13, 32133–32173, 2013

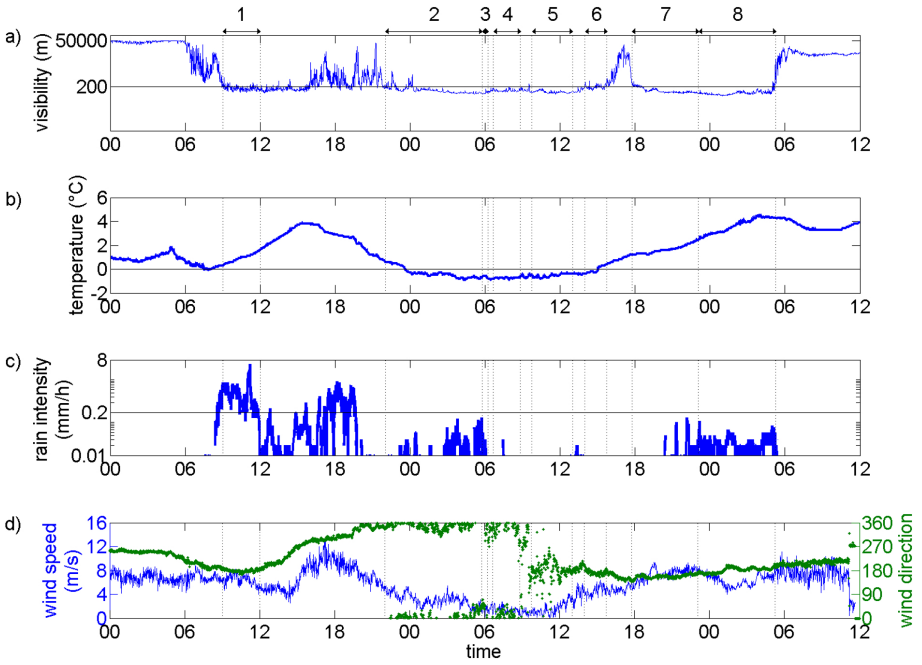

Fig. 5. Time series of weather parameters observed during the cloud event on 22–24 October 2011. **(a)** visibility, **(b)** temperature, **(c)** rain intensity, **(d)** wind speed (left axis) and direction (right axis). Different periods described in the text are marked with dashed lines and also with numbered arrows above **(a)** (1 = rainy, 2 = clean, 3 = paper mill, 4 = clean 2, 5 = heating plant, 6 = southern 1, 7 = southern 2, 8 = southern 3).

ACPD
13, 32133–32173, 2013

The effect of local sources on aerosol-cloud interactions

H. Portin et al.

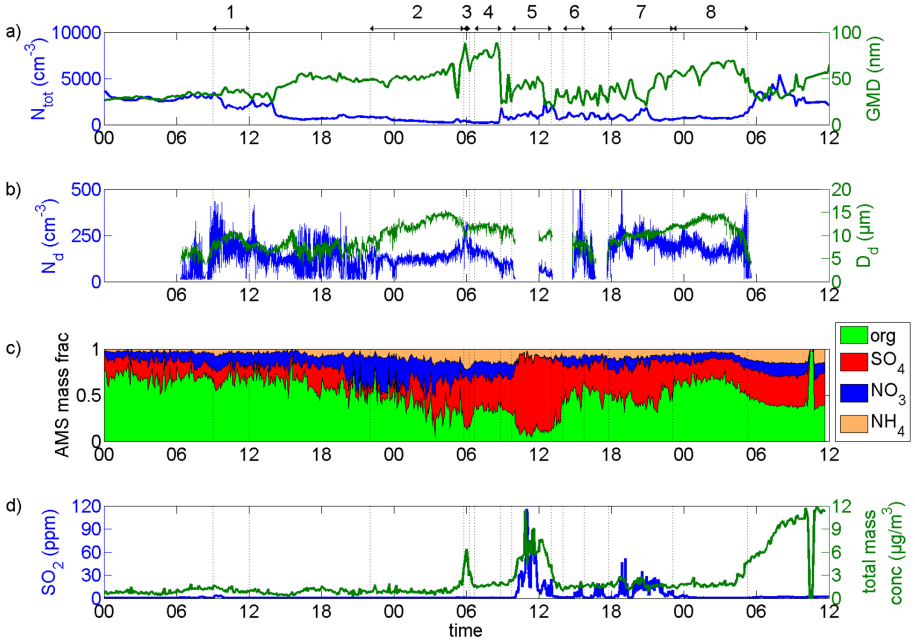

Fig. 6. Time series during the cloud event on 22–24 October 2011 of **(a)** total particle number concentration (left axis) and geometric mean particle diameter (right axis), **(b)** cloud droplet number concentration (left axis) and mean droplet diameter (right axis), **(c)** mass fractions of different chemical components measured by the AMS and **(d)** SO_2 concentration (left axis) and total particle mass concentration measured by the AMS (right axis). Different periods described in the text are marked with dashed lines and also with numbered arrows above **(a)** (1 = rainy, 2 = clean, 3 = paper mill, 4 = clean 2, 5 = heating plant, 6 = southern 1, 7 = southern 2, 8 = southern 3).

ACPD
13, 32133–32173, 2013

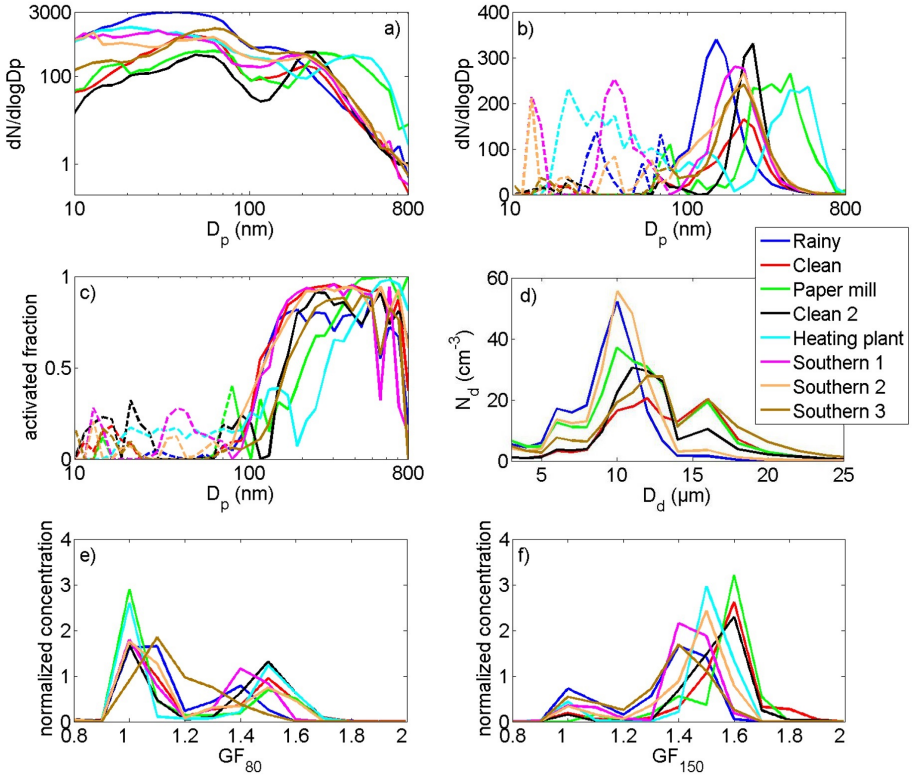

Fig. 7. (a) Total particle size distributions, **(b)** size distributions of activated particles, **(c)** activated fraction of particles as a function of particle diameter, **(d)** cloud droplet size distributions and growth factor distributions for **(e)** 80 nm and **(f)** 150 nm particles for the different periods of the cloud event observed on 22–24 October 2011. In **(b)** and **(c)** data for particles smaller than 80 nm in diameter are illustrated with dashed lines due to the inaccuracies discussed in the text. In **(e)** and **(f)** normalized concentration means that the integral of the particle concentrations over GF equals 100.

ACPD
13, 32133–32173, 2013

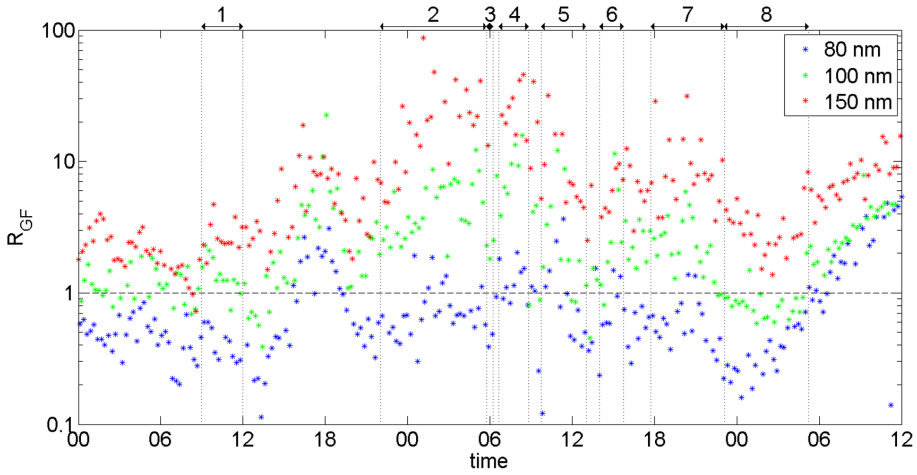

Fig. 8. Time series of the ratio between the number concentrations of more and less hygroscopic particles, $R_{GF} = N_{GF>1.25}/N_{GF\leq1.25}$ observed during the cloud event on 22–24 October 2011. Different periods described in the text are marked with dashed lines and also with numbered arrows (1 = rainy, 2 = clean, 3 = paper mill, 4 = clean 2, 5 = heating plant, 6 = southern 1, 7 = southern 2, 8 = southern 3).

ACPD
13, 32133–32173, 2013